Medical Oncology (2020) 37:98
https://doi.org/10.1007/s12032-020-01427-0

ORIGINAL PAPER

# The prostate-specific membrane antigen (PSMA)-targeted radiotracer $^{18}$F-DCFPyL detects tumor neovasculature in metastatic, advanced, radioiodine-refractory, differentiated thyroid cancer

**Prasanna Santhanam[1,5] · Jonathon Russell[2] · Lisa M. Rooper[3] · Paul W. Ladenson[1] · Martin G. Pomper[4] · Steven P. Rowe[4]**

Received: 19 June 2020 / Accepted: 26 September 2020 / Published online: 9 October 2020


## Abstract

Prostate-specific membrane antigen (PSMA; also termed glutamate carboxypeptidase II (GCP II)) is abundantly expressed in prostate cancer. It has been shown recently that PSMA is expressed in neovasculature of differentiated thyroid cancer. In this study, we show that $^{18}$F-DCFPyl might detect neovasculature in advanced, metastatic differentiated thyroid cancer (DTC). We first stained the preserved lymph node samples of three patients with DTC who had undergone total thyroidectomy and neck dissection for cervical lymph node metastatic disease to identify PSMA expression, with the PSMA antibody (DAKO Monoclonal). Then, we performed $^{18}$F-DCFPyl imaging in two other advanced DTC patients with elevated serum thyroglobulin (Tg), indicative of residual disease. We compared the findings with contemporaneous FDG PET/CT scan, conventional Imaging (CT,MRI) and whole-body scan performed with $I^{123}/I^{131}$. All the three lymph node samples stained positive for PSMA expression in the neovasculature. In the first imaged patient, $^{18}$F-DCFPyl detected activity within the retropharyngeal CT contrast-enhancing lymph node. Compared to FDG PET/CT, the $^{18}$F-DCFPyl scan showed a greater SUV (3.1 vs 1.8). In the second imaged patient, $^{18}$F-DCFPyl showed intense uptake in the L3 vertebra (not seen on the post treatment $^{131}$I scan or the $^{18}$F-FDG PET/CT). MRI of the lumbar spine confirmed the presence of sclerotic-lytic lesion at the location, consistent with metastatic disease. Our exploratory study is proof of principle, that the prostate cancer imaging agent $^{18}$F-DCFPyl may prove useful for the localization of metastases, in patients with metastatic RAI-refractory DTC by detecting neoangiogenesis within the tumor.

**Keywords** PSMA · 18F-DCFPyL · DTC · Tumor neovasculature

✉ Prasanna Santhanam
psantha1@jhmi.edu

1 Division of Endocrinology, Diabetes, & Metabolism, Department of Medicine, Johns Hopkins University School of Medicine, Baltimore, MD 21287, USA

2 Department of Otolaryngology – Head and Neck Surgery, Johns Hopkins University School of Medicine, Baltimore, MD 21287, USA

3 Division of Surgical Pathology, Department of Pathology, Johns Hopkins University School of Medicine, Baltimore, MD 21287, USA

4 Division of Nuclear Medicine, The Russell H. Morgan Department of Radiology and Radiological Science, Johns Hopkins University School of Medicine, Baltimore, MD 21287, USA

5 Division of Endocrinology, Metabolism and Diabetes, Johns Hopkins University School of Medicine, 5501 Hopkins Bayview Circle, Asthma and Allergy Center, suite 3 B 73, Baltimore, MD 21224, USA

## Introduction

Prostate-specific membrane antigen (PSMA; also termed glutamate carboxypeptidase II) is abundantly expressed in prostate cancer and is identical to the folate hydrolase I found in the jejunal brush border and the N-acetyl-alpha-linked-acidic-dipeptidase (NAALADase) in the nervous system [1].It is a type II transmembrane glycoprotein with an extracellular C-terminus and a cytoplasmic N-terminus such that the extracellular domain binds to N-acetyl aspartyl glutamate (NAAG) in the nervous system, where it hydrolyses NAAG to glutamate and *N*-acetyl aspartate, and to folyl-poly-γ glutamate in the jejunum, contributing to folate metabolism [1].

While PSMA is over-expressed on the epithelial tumor cells of prostate cancer, the expression is primarily on the endothelial cells of the neovasculature in many other solid

tumors including colon, breast and adrenocortical cancers [2, 3].In a study of 68 patients with 91 samples, which included 37 patients with differentiated thyroid cancers (DTCs), PSMA expression was graded on a score of no expression (score 0), weak (score 1–3), moderate [4–6] or strong expression [2, 7]; all classic papillary thyroid cancers (PTCs) and follicular thyroid cancers (FTCs) stained positive for PSMA. Sixty-four percent of PTCs stained moderate or strong and 45% of FTCs stained moderate or strong [2]. PSMA expression was seen in 100% of distant metastases and 67% of lymph node metastases [2].

In another recently published study, PSMA expression in the neovasculature was significantly more frequent in malignant tumors compared to benign tumors (36/63; 57.1% vs. 5/38; 13.2%; $p = 0.0001$) [4]. These studies imply that agents targeting PSMA might be useful in diagnostic and therapeutic targeting of advanced DTCs that exhibit significant neoangiogenesis.

Small-molecule radiopharmaceuticals using $^{18}$F are of immense value due to their inherent suitability for medical imaging owing to abundant positron production allowing for positron emission tomography (PET) imaging, the ease of synthetic accessibility, salutary pharmacokinetics, capacity for introduction to clinical workflow, and favorable imaging characteristics. The agent $^{18}$F-DCFPyl *(2-(3-{1-carboxy-5-[(6-[(18)F]fluoro-pyridine-3-carbonyl)-amino]-pentyl}-ureido)-pentane-dioic acid)* was developed at Johns Hopkins as a PSMA imaging agent. It displayed high affinity for PSMA (Ki $1.1 \pm 0.1$ nM), high radiochemical yield on synthesis (36–53%), and very favorable tissue distribution in both mice models and humans [5–7]. In 2011, a preclinical evaluation showed that $^{18}$F-DCFPyL had uptake in PSMA-positive prostate tumor xenografts and the uptake was significantly higher when compared to PSMA-negative tumors (358:1) at 2 h post injection [5]. In a 9-patient study, $^{18}$F-DCFPyL PSMA showed no safety issues in humans with highest dosimetry in kidneys and urinary bladder and substantial uptake in submandibular gland and liver [7].

No previous study has used the radiotracer $^{18}$F-DCFPyL for the imaging of DTC lesions prospectively. The aim of our study was to determine if $^{18}$F-DCFPyL PET/computed tomography (CT) improved the localization of DTC in patients with advanced thyroid cancer when compared to $^{131}$I post treatment scan and 2-deoxy-2-[$^{18}$F]fluoro-D-glucose ($^{18}$F-FDG) PET/CT as proof of principle. We also examined the degree and pattern of PSMA expression in stored histopathological samples of persons with advanced DTC.

## Research design and methods

This study was approved by our local Johns Hopkins Institutional Review Board (IRB) and ethics committee (Office of Human Research). Imaging with $^{18}$F-DCFPyL PET/CT was carried out under a United States Food and Drug Administration Investigational New Drug application (IND 121,064). Patients who underwent imaging signed informed consent. In this pilot study, we first examined the expression of PSMA in 3 patients (shown in Table 1) with DTC and cervical lymph node metastatic disease. All the patients had undergone total thyroidectomy with neck dissection for metastatic lymph nodes.

In each of the patients, we reviewed the electronic medical record and abstracted information including: demographics (age, gender, ethnicity, body mass index), history of presentation, physical examination, first ultrasound (US) of the thyroid (nodule size, shape, vascularity, echogenicity, presence of sonographic high-risk factors, e.g., microcalcifications), thyroid function tests, other imaging findings (US, CT, PET/CT), fine-needle aspiration (FNA) cytopathology results (based on revised Bethesda classification), preoperative US of the soft tissue and neck, extent of lymph node involvement by sonography and/or FNA cytology, other imaging findings, surgery performed (lobectomy vs total thyroidectomy), extent of neck dissection, final

**Table 1** The characteristics of patients whose lymph node samples were stained for PSMA expression in the neovasculature

| Patient | Age | Gender | Diagnosis | Extent of the disease | Lymph node involvement | Thyroglobulin(± Ab) | Comments |
|---|---|---|---|---|---|---|---|
| A | 60 | F | Papillary thyroid cancer with tall cell features | Involvement of cricoid cartilage, Extrathyroidal extension | Right Level 3,4, Midline Level 7 | 1.4 (−ve Ab) | LN Sample + for PSMA (Fig. 1a) |
| B | 46 | M | Classic papillary thyroid cancer | Multiple + lymph nodes central and left lateral neck | Left superior Level 6 | 2.6 (−ve Ab) | LN Sample + for PSMA (Fig. 1b) |
| C | 66 | M | Tall cell variant PTC | Positive margins, involvement of skeletal muscle | Right neck levels 2–5 | 2.8 (−ve Ab) | LN Sample + for PSMA (Fig. 1c) |

histopathological diagnosis, and tumor stage (8th edition TNM classification), complications during surgery, postoperative thyroglobulin levels, diagnostic $^{123}$I results, dose of $^{131}$I administered, post treatment scan results, post treatment thyroglobulin (± thyroglobulin antibody trend), as well as serial TSH-stimulated and suppressed thyroglobulin level(s).

The stored lymph node samples were stained with the DAKO monoclonal PSMA antibody. Monoclonal anti-PSMA clone 3E6 recognizes an epitope present in the 57–134 amino acid region of the extracellular portion of PSMA [8]. Monoclonal mouse anti-PSMA has been shown to react in Western blotting with PSMA from cell lysates, seminal fluid, and with recombinant baculovirus expressed PSMA [8]. When compared to the anti-endothelial cell antibody against CD34, the anti-PSMA antibody 7E11 has shown a pattern of staining primarily consistent with the neovascular distribution within a wide range of tumors [9]. The DAKO monoclonal PSMA antibody (catalog# M3620) clone 3E6 is a commercially available and validated assay for detection of PSMA expression [8, 10].The reagent is supplied by the manufacturer in a liquid form as tissue culture supernatant in 0.05 mol/L Tris–HCl, pH 7.2 and 0.015 mol/L sodium azide, containing a stabilizing protein [8]. In a previously described method, thick sections (5 µm) were deparaffinized by Histo-clear (www.nationaldiagnostics.com), incubated in a target-retrieval solution for 30 min, treated with peroxidase block (to block endogenous peroxidase activity) for 5 min, and then incubated with PSMA antibody for 60 min [2]. If areas of activity were seen on the slides, those samples were considered positive.

### Imaging protocol

Subsequently, we imaged 2 other patients with suspected DTC recurrence with $^{18}$F-DCFPyL. A bolus of less than or equal to 9 mCi (333 MBq) of $^{18}$F-DCFPyL was given intravenously (IV). The mass dose of $^{18}$F-DCFPyL administered was less than 3.98 µg per patient. PET/CT was performed on a Discovery DRX PET/CT scanner (GE Healthcare, Waukesha, WI, USA) or Biograph mCT PET/CT (Siemens Healthineers, Erlangen, Germany) operating in 3-dimensional emission acquisition mode and with attenuation correction via low dose CT. Patients were scanned in the supine position starting from the mid-thigh to the vertex of skull approximately 60 min after radiotracer injection. The scan included 7 to 9 fields-of-view, depending on patient height. An initial low dose x-ray CT transmission scan, preceding the PET emission acquisition, was used for tissue attenuation correction and anatomical correlation.

## Results

The characteristics and findings of the three participants with histopathological examination is shown in Table 1. The three participants had findings of non-RAI (Radioiodine) avid residual disease. Patient A—had an FDG avid right cervical level 3 lymph node and a sub-centimeter-sized right lung nodule that did not show any radiotracer uptake on the iodine based WBS (Whole-Body Scan). Patient B—had uptake in the thyroid bed but no evidence of extrathyroidal uptake (especially in the resected lymph node sample that was compatible with non-RAI disease). Patient C- had multiple pulmonary nodules on CT scan of the chest that were not RAI avid (negative WBS) but likely represented advanced residual disease.

The pathology slides are shown in Fig. 1a–c. All the patients in Group I showed expression of PSMA in the neovasculature. However, none of the thyroid follicular cells stained positive for PSMA.

The characteristics of the participants (including age, subtype of DTC as well as unstimulated Thyroglobulin ($T_g$) at the time of imaging) who underwent the $^{18}$F-DCFPyL PET CT research scan is shown in Table 2. Of note, $T_g$ levels in the patients imaged by the $^{18}$F-DCFPyL PET CT were significantly higher than in patients whose lymph nodes were stained with DAKO PSMA antibody (Tables 1 and 2).

The first imaged patient (ID # 1) had no uptake on the diagnostic $^{123}$I diagnostic whole-body scan (WBS) while the contrast-enhanced CT scan showed a retropharyngeal

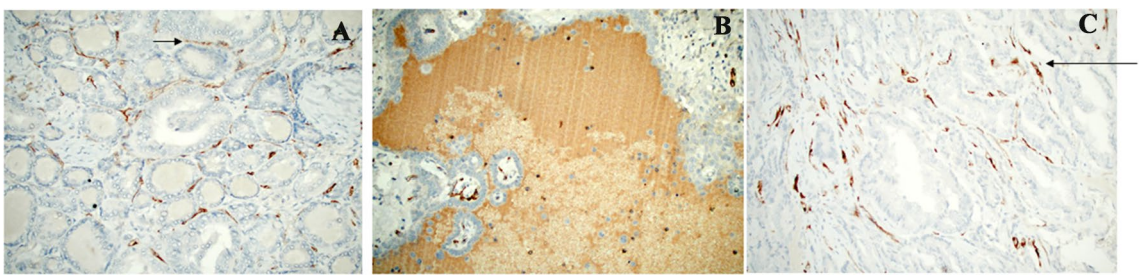


**Fig. 1** **a–c** The stored LN samples were stained with DAKO Monoclonal anti-PSMA Antibody clone 3E6 that recognizes an epitope present in 57–134 amino acid region. All the three LN samples stained positive for GCP-II (PSMA) shown by line arrows

lymph node with abnormal enhancement (Table 3). This lymph node showed minimal, if any, uptake on the $^{18}$F-FDG PET/CT but more convincing increased uptake (although still only mild) on the $^{18}$F-DCFPyL PET/CT. The maximum standardized uptake value ($SUV_{max}$) was 3.1 with $^{18}$F-DCFPyL but only 1.8 on the $^{18}$F-FDG PET (Fig. 2).

The second patient (ID # 2), who underwent imaging, had mild elevation of Tg and was found to have left sided 0.9 cm lung nodule on CT chest that was radioiodine (RAI)-avid on the diagnostic $^{123}$I scan as well as the post treatment scan (Table 3). The $^{18}$F-FDG PET/CT had shown low level of uptake in the lung nodule. $^{18}$F-DCFPyL showed intense uptake in the anterior aspect of L3 ($SUV_{max}$ 7.9) not seen on the post treatment $^{131}$I scan or the $^{18}$F-FDG PET/CT ($SUV_{max}$ in this region was 2.2 and visibly the same as background blood pool or marrow). Magnetic resonance imaging (MRI) of the lumbar spine confirmed the presence of an 8-mm mixed sclerotic-lytic lesion at the same location, with enhancement and surrounding bone marrow edema, highly suggestive of metastatic disease (Fig. 3). Of note, the radioiodine-avid lung nodule did not have uptake of $^{18}$F-DCFPyL. Figure 4 shows the MIP images of $^{18}$F-FDG-PET CT and $^{18}$F-DCFPyL PET/CT of the two imaged patients. The cervical lymph node is not discernable in these images as this

**Table 2** Characteristics of the patients who were imaged by $^{18}$F-DCFPyL

| Patient ID | Age | Gender | Diagnosis | Extent of the disease at presentation | Lymph node involvement | Thyroglobulin(± Ab) |
|---|---|---|---|---|---|---|
| 1 | 38 | M | Classic PTC | Multifocal with angioinvasion and Lymphatic Invasion | left Neck Levels 1–5 | 13.4 (−ve Ab) |
| 2 | 59 | M | Follicular thyroid cancer | Minimal invasion measuring 3.5 cm | N/A | 12.9 (−ve Ab) |

**Table 3** Summarizes the Imaging findings of the two patients

| Patient ID | Conventional imaging | NM Thyroid scan | 18F-FDG PET CT | 18F-DCFPyL |
|---|---|---|---|---|
| 1 | CT neck<br>An enhancing ovoid right lateral retropharyngeal LN (0.9 cm) | Diagnostic I-123 scan<br>No focal areas of increased radiotracer uptake s/o local or regional metastasis | Foci of non-specific uptake in Neck | Increased DCFPyL uptake noted in the Retropharyngeal LN |
| 2 | CT chest<br>0.9 cm left upper lobe solid nodule<br>0.5 cm right lower lobe solid nodule<br>MRI<br>Ill-defined small 8 mm lesion in the anterior aspect of L3 vertebral body, with no loss of signal in out of phase images | Post treatment<br>I-131 scan<br>Intense uptake noted in the left upper pole nodule | 1.1 × 1.1 cm left upper lobe solid nodule with mild FDG Uptake | No uptake seen in the lung lesion<br>The mixed lytic/sclerotic lesion at the right anterior L3 shows intense DCFPyL uptake |

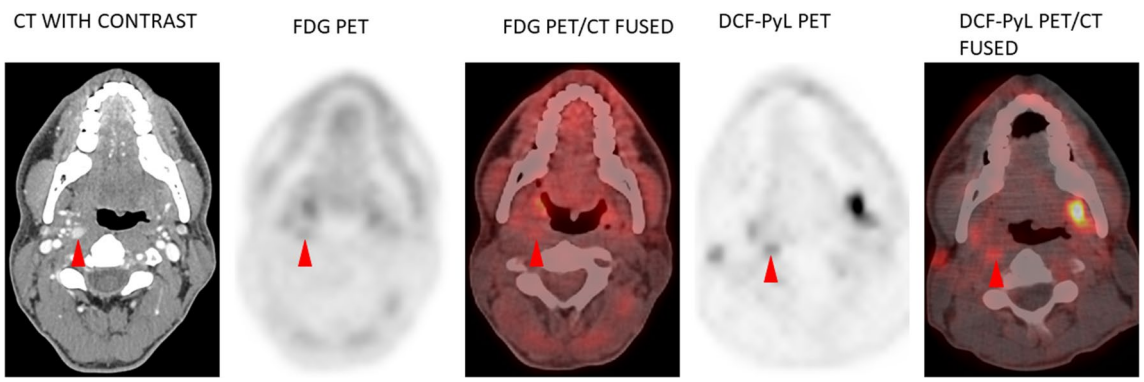


**Fig. 2** Patient 1 – Molecular Imaging shows increased Radiotracer Uptake in the Retropharyngeal Lymph Node with an increased SUV. DCF-PyL PET Shows an SUV of 3.1 compared to FDG-PET that shows an SUV of 1.8

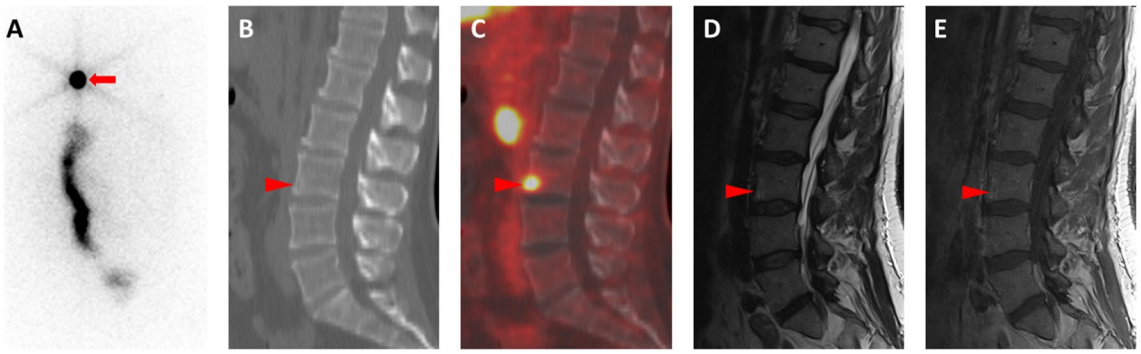


**Fig. 3** (Patient 2) **a** Posterior planar whole-body $^{131}$I post-therapy scan shows evidence of lung metastases (red arrow) and physiologic bowel uptake, but no abnormal uptake in the region of the lumbar spine. **b** Sagittal CT image through the lumbar spine demonstrating subtle rarefaction of the anterior aspect of the L3 vertebral body (red arrowhead). **c** Sagittal fused $^{18}$F-DCFPyL PET/CT image shows that there is intense radiotracer uptake at the same location (red arrowhead). **d** Sagittal T2-weighted and **e** sagittal T1-weighted post-contrast magnetic resonance images show perilesional edema (red arrowhead in (**d**)) and subtle enhancement (red arrowhead in (**e**)), confirming the presence of the lesion seen on PET

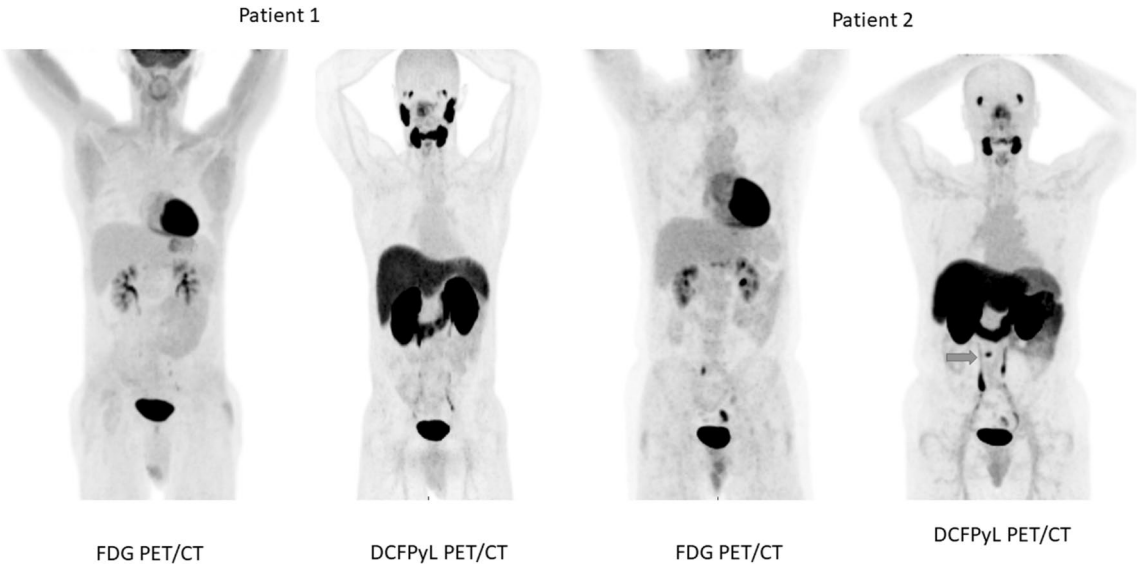


**Fig. 4** MIP images of FDG-PET CT and $^{18}$F-DCFPyL PET/CT of the two imaged patients. The cervical retropharyngeal lymph node is not discernable in these pictures as this was seen mostly in the cross-sectional images (Patient 1). The small vertebral metastatic lesion is shown by the blue arrow (Patient 2)

was best appreciated in the cross-sectional images (Patient 1). The small vertebral metastatic lesion is shown by the blue arrow (Patient 2).

## Discussion

Most cases of DTC have excellent prognosis following lobectomy/ total thyroidectomy with and without radioiodine treatment and the surveillance usually involves measurement of $T_g$ on levothyroxine, neck US and CT, and occasionally $^{18}$F-FDG PET/CT [11]. However, a small percentage of DTCs are aggressive with poor prognosis. Post treatment (surgery ± radioiodine therapy), unstimulated or stimulated $T_g$ values greater than 10–30 ng/mL increase the likelihood of having persistent or recurrent disease, RAI-refractory disease, distant metastases, and increased mortality [12]. As was evident in our imaged patients, clinically localizing disease in patients with aggressive DTC poses a distinct challenge.

PSMA is a 100 kDa type II transmembrane protein (belonging to the M28 peptidase family) with folate hydrolase and NAALAdase activity [13]. FOLH1, the gene that encodes the protein, consists of 19 exons spanning approximately 60 kb of genomic DNA [13]. The genetic structure is shown in Fig. 5 (adapted from https://www.genecards.

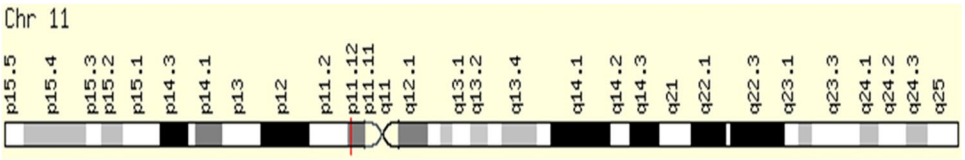


**Fig. 5** Genomic Locations for FOLH1 Gene *chr11:49,145,092–49,208,670,* (GRCh38/hg38) ( Source www.genecards.org)

org). In a study by Silver et al. in 1997, PSMA expression in neovascular endothelium of tumors was a novel finding, while studying the immunohistochemical analysis performed on different extra-prostatic tissues, the implications of which was unclear at that time [14]. Its expression seems to be similar to another enzyme, CD13 (also known as Aminopeptidase N, a zinc metalloproteinase) [15, 16]. Chang et al., evaluated five different monoclonal antibodies against PSMA and showed that the protein is expressed in a wide range of tumors in the associated neovasculature (including renal cell carcinoma, colonic adenocarcinoma, and malignant melanoma) [9].

Conway et al. showed that PSMA is essential for endothelial invasion through in vitro studies that showed the protein participates in laminin-specific integrin signaling via the Rho GTPase effector molecule p21-activated kinase 1 (PAK-1) [16]. PSMA (in association with matrix metalloprotease-2) appears to produce small laminin peptide fragments (containing carboxy-terminal glutamate moieties) that increase endothelial cell adhesion, and activate integrin α6 β1 and focal adhesion kinase [17, 18]. These findings suggest the reason for PSMA expression in tumor neovascular endothelium. Regardless of the mechanism by which PSMA is expressed on the neovasculature of most solid tumors, its presence indicates a potential role for PSMA-based diagnostic and therapeutic (i.e. theranostic) agents in the management of a wide range of tumors targeting the critical angiogenesis component of tumor proliferation.

Recently, it was shown by Sollini et al., that in a multivariate regression model to predict RAI-refractoriness, the stage of the disease, the degree of PSMA expression if high (≥ 80%), and the interaction between moderate PSMA expression (11–79%) and stage were the most important covariates [19]. PSMA expression was strongly associated with tumor aggressiveness and poor patient outcomes [19].

$^{131}$I Negative DTC was first detected by a PSMA-based PET radiotracer, $^{68}$ Ga-PSMA-11, which showed uptake in a cervical lymph node and pulmonary metastasis [20]. Subsequently, another patient with rising thyroglobulin and negative $^{131}$I whole-body scan had intense $^{68}$ Ga-PSMA-11 uptake in mediastinal and left supraclavicular lymph nodes, brain, pulmonary nodules, and skeletal sites [21]. There have also been reports of incidental thyroid uptake of $^{68}$ Ga -PSMA-11 in a follicular adenoma when the patient was being investigated for prostate cancer [22]. Beyond those studies, our results would suggest that PSMA expression in DTC tumor-associated neovasculature may be heterogenous, given that the second imaged patient had intense $^{18}$F-DCFPyL uptake in a spinal metastasis but lacked uptake in a lung metastasis that was positive on $^{131}$I post treatment scan. The exact utility of PSMA-targeted radiotracers and the ideal clinical scenarios in which they should be used for DTC will require further study. Furthermore, obtaining a tissue diagnosis post $^{18}$F-DCFPyL imaging is the next logical step in further consolidating evidence for this image modality.

PSMA-based radiotracers, especially those incorporating $^{18}$F, which has significant practical and image-quality advantages relative to $^{68}$ Ga, have not been comprehensively evaluated in advanced thyroid cancer [23, 24]. Our proof of principle study shows significantly increased neovascular PSMA expression in lymph nodes of DTC as well as the ability of $^{18}$F-DCFPyL to detect lesions that were previously unnoticed by RAI-based imaging as well as $^{18}$F-FDG PET/CT.

Given the above evidence of PSMA expression and imaging in advanced DTC, our research premise appears promising. In our patients, RAI-refractory disease was successfully imaged and detected by $^{18}$F-DCFPyL. Further prospective studies are needed in this regard.

**Funding** Funding was received from the Prostate Cancer Foundation Young Investigator Award and National Institutes of Health Grants CA134675, CA184228, EB024495, and CA183031.

## Compliance with ethical standards

**Conflict of interest** Prasanna Santhanam**,** Jonathon Russell, Lisa M Rooper, and Paul W. Ladenson have no conflict of interest /disclosures to report. Martin. G. Pomper is a coinventor on a US patent covering 18F-DCFPyL and as such is entitled to a portion of any licensing fees and royalties generated by this technology. This arrangement has been reviewed and approved by the Johns Hopkins University in accordance with its conflict of interest policies. He has received research funding through Progenics Pharmaceuticals. Steven. P. Rowe is a consultant for Progenics Pharmaceuticals, Inc., the licensee of 18F-DCFPyL. He has received research funding from Progenics Pharmaceuticals, Inc.

## References

1. Ristau BT, O'Keefe DS, Bacich DJ. The prostate-specific membrane antigen: lessons and current clinical implications from 20 years of research. Urol Oncol. 2014;32(3):272–9.

2. Moore M, Panjwani S, Mathew R, Crowley M, Liu YF, Aronova A, et al. Well-differentiated thyroid cancer neovasculature expresses prostate-specific membrane antigen-a possible novel therapeutic target. Endocr Pathol. 2017;28(4):339–44.
3. Salas Fragomeni RA, Amir T, Sheikhbahaei S, Harvey SC, Javadi MS, Solnes LB, et al. Imaging of nonprostate cancers using PSMA-targeted radiotracers: rationale, current state of the field, and a call to arms. J Nucl Med. 2018;59(6):871–7.
4. Heitkotter B, Steinestel K, Trautmann M, Grunewald I, Barth P, Gevensleben H, et al. Neovascular PSMA expression is a common feature in malignant neoplasms of the thyroid. Oncotarget. 2018;9(11):9867–74.
5. Chen Y, Pullambhatla M, Foss CA, Byun Y, Nimmagadda S, Senthamizhchelvan S, et al. 2-(3-{1-Carboxy-5-[(6-[18F]fluoro-pyridine-3-carbonyl)-amino]-pentyl}-ureido)-pen tanedioic acid, [18F]DCFPyL, a PSMA-based PET imaging agent for prostate cancer. Clin Cancer Res. 2011;17(24):7645–53.
6. Rowe SP, Gorin MA, Pomper MG. Imaging of prostate-specific membrane antigen using [(18)F]DCFPyL. PET Clin. 2017;12(3):289–96.
7. Szabo Z, Mena E, Rowe SP, Plyku D, Nidal R, Eisenberger MA, et al. Initial evaluation of [(18)F]DCFPyL for prostate-specific membrane antigen (PSMA)-targeted PET imaging of prostate cancer. Mol Imag Biol. 2015;17(4):565–74.
8. Murphy GPBA, Holmes EH, Tino WT (2000) Monoclonal antibodies specific for the extracellular domain of prostate-specific membrane antigen. *United States Patent 6,150,508.*
9. Chang SS, Reuter VE, Heston WD, Bander NH, Grauer LS, Gaudin PB. Five different anti-prostate-specific membrane antigen (PSMA) antibodies confirm PSMA expression in tumor-associated neovasculature. Can Res. 1999;59(13):3192–8.
10. Inc AT. Monoclonal Mouse Anti-Human ,Prostate-Specific Membrane Antigen (Concentrate) Clone 3E6 https://www.agilent.com/en/product/immunohistochemistry/antibodies-controls/primary-antibodies/prostate-specific-membrane-antigen-(concentrate)-76591. 2020.
11. Santhanam P, Ladenson PW. Surveillance for differentiated thyroid cancer recurrence. Endocrinol Metab Clin North Am. 2019;48(1):239–52.
12. Haugen BR, Alexander EK, Bible KC, Doherty GM, Mandel SJ, Nikiforov YE, et al. 2015 American thyroid association management guidelines for adult patients with thyroid nodules and differentiated thyroid cancer: the american thyroid association guidelines task force on thyroid nodules and differentiated thyroid cancer. Thyroid. 2016;26(1):1–133.
13. O'Keefe DS, Su SL, Bacich DJ, Horiguchi Y, Luo Y, Powell CT, et al. Mapping, genomic organization and promoter analysis of the human prostate-specific membrane antigen gene. Biochem Biophys Acta. 1998;1443(1–2):113–27.
14. Silver DA, Pellicer I, Fair WR, Heston WD, Cordon-Cardo C. Prostate-specific membrane antigen expression in normal and malignant human tissues. Clin Cancer Res. 1997;3(1):81–5.
15. Schreiber CL, Smith BD. Molecular imaging of aminopeptidase N in cancer and angiogenesis. Contrast Media Mol Imaging. 2018;2018:5315172.
16. Conway RE, Petrovic N, Li Z, Heston W, Wu D, Shapiro LH. Prostate-specific membrane antigen regulates angiogenesis by modulating integrin signal transduction. Mol Cell Biol. 2006;26(14):5310–24.
17. Conway RE, Joiner K, Patterson A, Bourgeois D, Rampp R, Hannah BC, et al. Prostate specific membrane antigen produces pro-angiogenic laminin peptides downstream of matrix metalloprotease-2. Angiogenesis. 2013;16(4):847–60.
18. Conway RE, Rojas C, Alt J, Novakova Z, Richardson SM, Rodrick TC, et al. Prostate-specific membrane antigen (PSMA)-mediated laminin proteolysis generates a pro-angiogenic peptide. Angiogenesis. 2016;19(4):487–500.
19. Sollini M, di Tommaso L, Kirienko M, Piombo C, Erreni M, Lania AG, et al. PSMA expression level predicts differentiated thyroid cancer aggressiveness and patient outcome. EJNMMI Res. 2019;9(1):93.
20. Verburg FA, Krohn T, Heinzel A, Mottaghy FM, Behrendt FF. First evidence of PSMA expression in differentiated thyroid cancer using [(6)(8)Ga]PSMA-HBED-CC PET/CT. Eur J Nucl Med Mol Imaging. 2015;42(10):1622–3.
21. Taywade SK, Damle NA, Bal C. PSMA expression in papillary thyroid carcinoma: opening a new horizon in management of thyroid cancer? Clin Nucl Med. 2016;41(5):e263–e265265.
22. Sager S, Vatankulu B, Uslu L, Sonmezoglu K. Incidental detection of follicular thyroid carcinoma in 68Ga-PSMA PET/CT imaging. J Nucl Med Technol. 2016;44(3):199–200.
23. Sanchez-Crespo A. Comparison of Gallium-68 and Fluorine-18 imaging characteristics in positron emission tomography. Appl Radiat Isot. 2013;76:55–62.
24. Carter LM, Kesner AL, Pratt EC, Sanders VA, Massicano AVF, Cutler CS, et al. The impact of positron range on PET resolution, evaluated with phantoms and PHITS Monte Carlo simulations for conventional and non-conventional radionuclides. Mol Imag Biol. 2020;22(1):73–84.